Interaction Notes

Note 230

14 February 1975

Calculation of Currents Induced on a Disk by a Wire Grid Code

J. P. Castillo
K. C. Chen
B. K. Singaraju
Air Force Weapons Laboratory

Abstract

A wire grid model is critically studied based on a circular disk of radius $\lambda/20$ and $\lambda/2$. It is shown that the use of wires with small radii could lead to significant errors in the calculations of current densities. Comparisons with results using a body of revolution method are presented.

I. Introduction

The epidemic use of wire grid codes in the EMP community warrants a critical study of their validity. Historically, the wire grid code was first applied to the RCS calculations of the complicated objects, such as an aircraft or a Chinook helicopter.[1,2] The results obtained for RCS analysis compare well with the measurements. In recent years, thin wire modeling of aircraft, etc., has become very popular for calculating the skin current.

An extensive survey of thin wire codes is discussed in a report by Miller, et al.[3] Thin wire codes have been extended to calculate the current on a solid body by approximating the solid surface by a wire grid. Curtis, et al., of The Boeing Company have used the wire grid codes to calculate the current on a solid surface.[4,5] It is the purpose of this report to examine the results of this wire grid code. Toward this end, we compare the results for a solid perfectly conducting circular disk[6,14] with those obtained from the wire grid code.[4.5]

In this report we consider a plane wave incident on a flat circular disk. The electric field vector is polarized along the X-axis as shown in figure 6 with normal incidence. Results for this polarization are shown in figures 2 through 5.

II. Comparison of the Results

A perfectly conducting thin disk of 30 m diameter was modeled by a wire grid as shown in figure 1. The wire grid code supplied by Curtis has been used to calculate the currents. Comparisons are made with the results obtained by Lee[13] and by Graves, et al.[14] for a perfectly conducting disk and are as follows:

1. Effect of the Wire Radius on the Results

The currents obtained by the wire grid code are averaged by defining a current density J_i given by

$$J_i = \frac{I_i}{d_i} \tag{1}$$

where I_i is the current at the center of the i^{th} wire element and d_i is as shown in figure 1. This procedure merely distributes the current in the i^{th} element over a finite region. Comparisons are made for the normalized radial and azimuthal currents with the results for a solid disk. The wire radii are varied from 2.12×10^{-4} m to 2.12×10^{-2} m and the results are compared for $\lambda = 300$ m and a disk radius of $\lambda/20$ as shown in figures 2 and 3, and for $\lambda = 30$ m as shown in figures 4 and 5 for disk radius $\lambda/2$. Notice that, as expected, the current varies considerably (approximately by a factor of 2) as the wire radius varies. Unless a criterion to determine the wire radius is available, the current obtained from the wire grid model is likely to be in error. Curtis[11] has found that the grid size to wire radius ratio should be approximately 15 to 25 for calculating echo area. Jones[12] as well as Lee[13] have stated that a wire radius ranging from 10^{-3} to 5×10^{-3} will cause the numerical results to vary by a factor of 4. Grid size is also important. Again Jones[12] points out that the grid should not exceed $\lambda/20$. Therefore, the question of optimum radius and grid size must be answered.

While radar cross section (RCS) is not of importance in the study of EMP it is instructive to compare the radar cross section obtained by several techniques as provided in table 1. The results of the radar cross section calculation vary by about a factor of 2 as the wire radius varies from 2.12×10^{-2} m to 2.12×10^{-4} m. The RCS results[6,7,8] obtained by wire grid codes appear to agree better with the measured data for solid plates as the wire radius increases.

2. Effective Radius

It has been shown by many authors that in the static approximation, an equivalence exists between wires and strips.[9] For instance, a wire

Harrington		Curtis	
	$a_w = 2.12 \times 10^{-2}$ m	$a_w = 2.12 \times 10^{-3}$ m	$a_w = 2.12 \times 10^{-4}$ m
$5\lambda^2$	$3.866\lambda^2$	$2.502\lambda^2$	$1.613\lambda^2$

Table 1. RCS Comparison of Curtis and Harrington for a Disk of Radius 15 m ($2\lambda/5$), λ = 37.5 m

of radius "a" is equivalent to a thin strip of width "4a." However, this approximation breaks down as the frequency increases. The solid surface of the scatterer can be considered to be made up of thin metallic strips which can be approximated by wires thus arriving at a wire model for the solid scatterer.

This approximation is only as good as the equivalence between wires and strips. As a consequence, unless an astronomical number of wires with spacing 4a between the wires are used in the wire grid code, such an equivalence cannot be achieved and the code is likely to be in error. Furthermore, this equivalence does not apply to wires closely spaced.

3. Polarization

No attempt was made to vary the polarization of the incident wave. The particular geometry selected (figure 1) will probably yield different results for different incident polarizations. A better geometry for the circular disk would probably be a radial-circumferential grid. It is not clear at this time how one would select the grid configuration for complicated scatterers. Lin[15] has found that the RCS for an aircraft does not agree as well with experimental data for polarization perpendicular to the fuselage as it does for polarization parallel to the fuselage.

III. Summary

A critical study of a wire grid code has been made based on the known results for the circular disk. Of particular importance is the dependence of current densities on the disk and RCS on the wire radius even for relatively small disks (i.e., radii of the disk = $\lambda/20$). Intuitively the wire grid disk can be considered as an impedance loaded disk with its impedance dependent upon the wire radius. It is clear that such an impedance loaded disk gives different results for different radii. It is also obvious that the same conclusion applies to all wire grid codes.

It is apparent that more work must be done analytically and experimentally so that a better understanding of the relationship between wire grid and solid surface current densities and the resulting limitations may be obtained. Numerical results must be explained through physical reasoning.

IV. Appendix

To better understand the problem of a circular disk, we include an appendix[10] to show the current densities for two different polarizations of incident waves. These are reproduced in figures 6 and 7. It is shown that for $\vec{k}$ and $\vec{E}$ parallel to the disk J_ϕ includes a term which is non-zero in the static limit. The equations used in the low frequency limit are:

Broadside Incidence:

$$\vec{E}^{inc} = \vec{e}_x E_o e^{-ikz}$$

$$\vec{H}^{inc} = -\vec{e}_y H_o e^{-ikz}, \quad E_o = Z_o H_o, \quad Z_o = 120\pi$$

$$J_\rho = \frac{-iE_o}{Z_o} \cdot \frac{2a}{\lambda} \cdot \frac{16}{3} \sqrt{1 - (\rho/a)^2} \cos\phi$$

$$= \frac{-iE_o}{Z_o} \cdot \frac{2a}{\lambda} F_\rho \cos\phi$$

$$J_\phi = \frac{iE_o}{Z_o} \cdot \frac{2a}{\lambda} \cdot \frac{16}{3} \frac{1 - \frac{1}{2}(\rho/a)^2}{\sqrt{1 - (\rho/a)^2}} \sin\phi$$

$$= \frac{iE_o}{Z_o} \cdot \frac{2a}{\lambda} F_\phi \sin\phi$$

Grazing Incidence:

$$\vec{E}^{inc} = \vec{e}_y E_o e^{ikx}$$

$$\vec{H}^{inc} = \vec{e}_z H_o e^{ikx}, \quad E_o = Z_o H_o$$

$$J_\rho = \frac{-iE_o}{Z_o} \cdot \frac{2a}{\lambda} \cdot \frac{8}{3} \sqrt{1 - (\rho/a)^2} \sin\phi$$

$$= \frac{-iE_o}{Z_o} \cdot \frac{2a}{\lambda} G_\rho \sin\phi$$

$$J_\phi = \frac{-E_o}{Z_o} \cdot \frac{4}{\pi} \frac{\rho/a}{\sqrt{1 - (\rho/a)^2}} + \frac{-iE_o}{Z_o} \cdot \frac{2a}{\lambda} \cdot \frac{8}{3} \frac{1 + (\rho/a)^2}{\sqrt{1 - (\rho/a)^2}} \cos\phi$$

$$= \frac{-E_o}{Z_o} G_\phi^o + \frac{-iE_o}{Z_o} \cdot \frac{2a}{\lambda} G_o^1 \cos\phi$$

with the time convention $e^{-i\omega t}$.

References

1. Knepp, D. L. (1971), Numerical Analysis of Electromagnetic Radiation Properties of Smooth Conducting Bodies of Arbitrary Shape in the Presence of Known External Sources, Ph.D. Dissertation, University of Pennsylvania.

2. Miller, E. K., and B. J. Maxum (1970), "Mathematical Modeling of Aircraft Antennas and Supporting Structure," Final Report, ECOM Contract ADDB07-68-0456, Report No. ECOM-0456-1.

3. Miller, E. K., et al. (1974), "An Evaluation of Computer Programs Using Integral Equations for the Electromagnetic Analysis of Thin Wire Structures," AFWL Interaction Notes, Note No. 177.

4. Lin, J. L., W. L. Curtis, and M. C. Vincent, "On the Field Distribution of an Aperture," IEEE Transactions on Antennas and Propagation, Vol. AP-22, No. 3, May 1974.

5. Lin, J. L., W. L. Curtis, and M. C. Vincent, "Radar Cross Section of a Conducting Plate by Wire Mesh Modeling," presented at 1973 IEEE International Symposium on Antennas and Propagation, Boulder, Colorado, August 1973.

6. Harrington, R. F., and J. R. Mautz (1969), "Radiation and Scattering from Bodies of Revolution," AFWL Interaction Notes, Note No. 188.

7. Mittra, R. (ed.) (1973), Computer Techniques in Electromagnetics, Pergamon Press.

8. Miller, E. K., and F. J. Deadrick, "Some Computational Aspects of Thin Wire Modeling," AFWL Interaction Notes, Note No. 153.

9. King, R. W. P. (1956), The Theory of Linear Antennas, Harvard University Press.

10. Lee, K. S. H., private communication.

11. Curtis, W. L., The Effect of Wire-Radius on Wire Mesh Models, private communication.

12. Jones, D. S., "Numerical Methods for Antenna Problems," Proceedings IEEE, Vol. 121, No. 7, July 1974.

13. Lee, K. S. H., private communication.

14. Graves, B. D., T. T. Crow, and C. D. Taylor, "On the Electromagnetic Field Penetration Through Apertures," AFWL Interaction Note 199, August 1974.

15. Lin, Y. T. (1972), Computation of Low Frequency Scattering from Airplanes, Ohio State University ElectroScience Laboratory Report 2768-9.

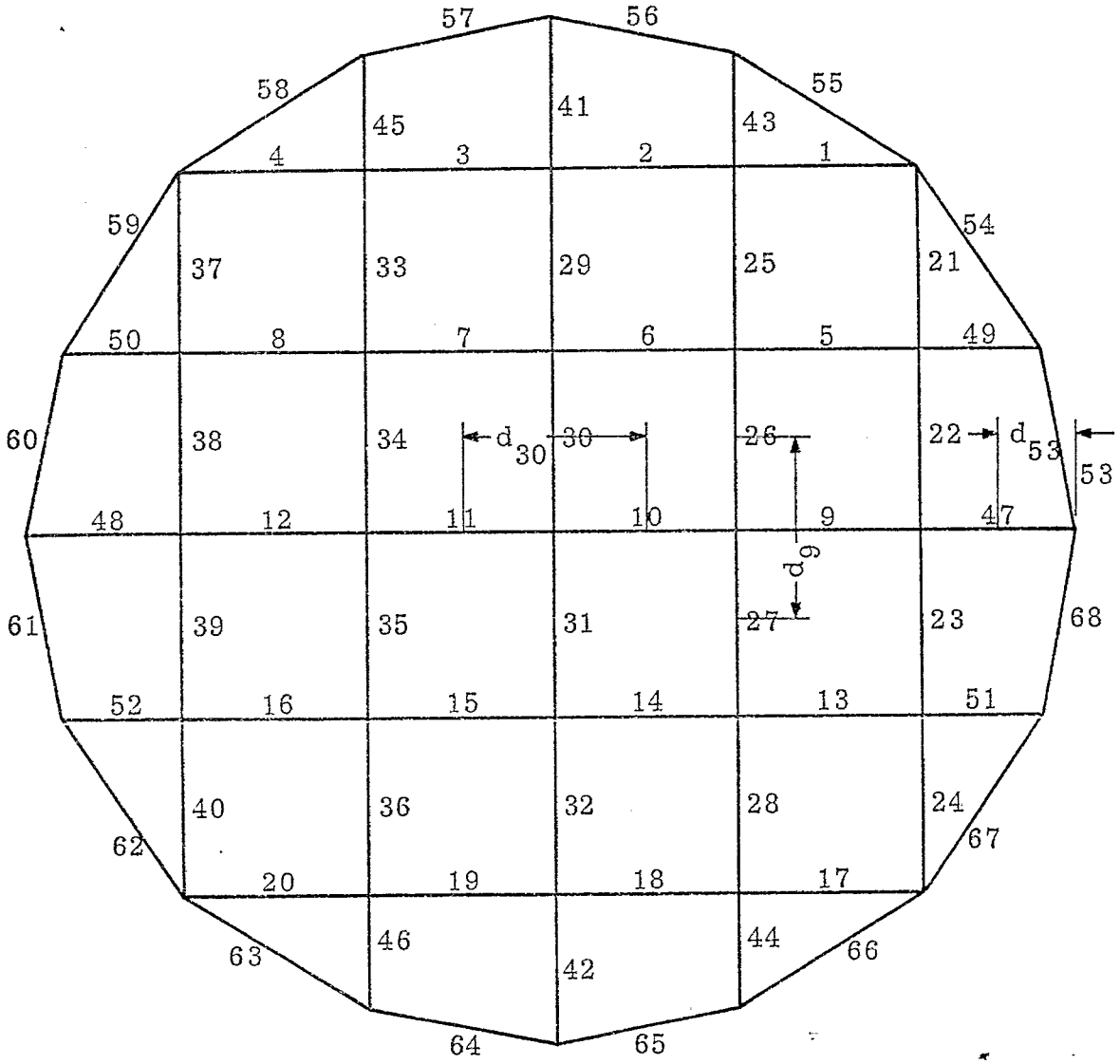

$\ell_1 = \ell_2 = \cdots = \ell_{40} = 5.3$ m $\qquad d_9 = d_{30} = 5.3$ m

$\ell_{41} = \ell_{42} = \ell_{47} = \ell_{48} = 4.4$ m $\qquad d_{53} = 2.2$ m

$\ell_{43} = \ell_{44} = \ell_{45} = \ell_{46} = \ell_{49} = \ell_{51} = \ell_{52} = \ell_{50} = 3.4$ m

Figure 1. Wire Grid Model of a Circular Disk

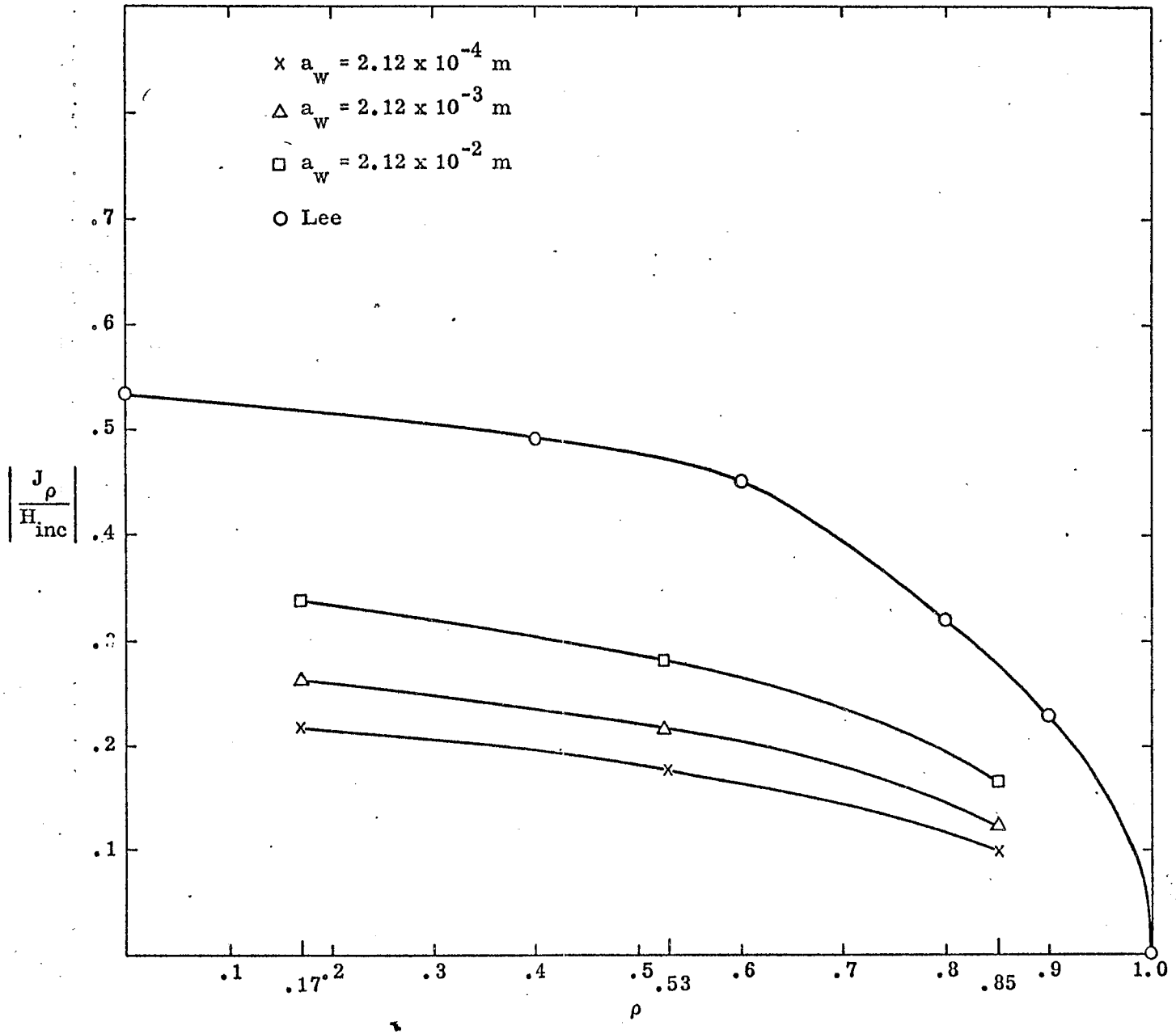

Figure 2. Normalized Radial Current Densities vs Distance from the Center of the Disk of 15 Meters Radius ($\lambda/20$) (λ = 300 meters; ρ is the normalized radius of the disk) for $\phi = 0$

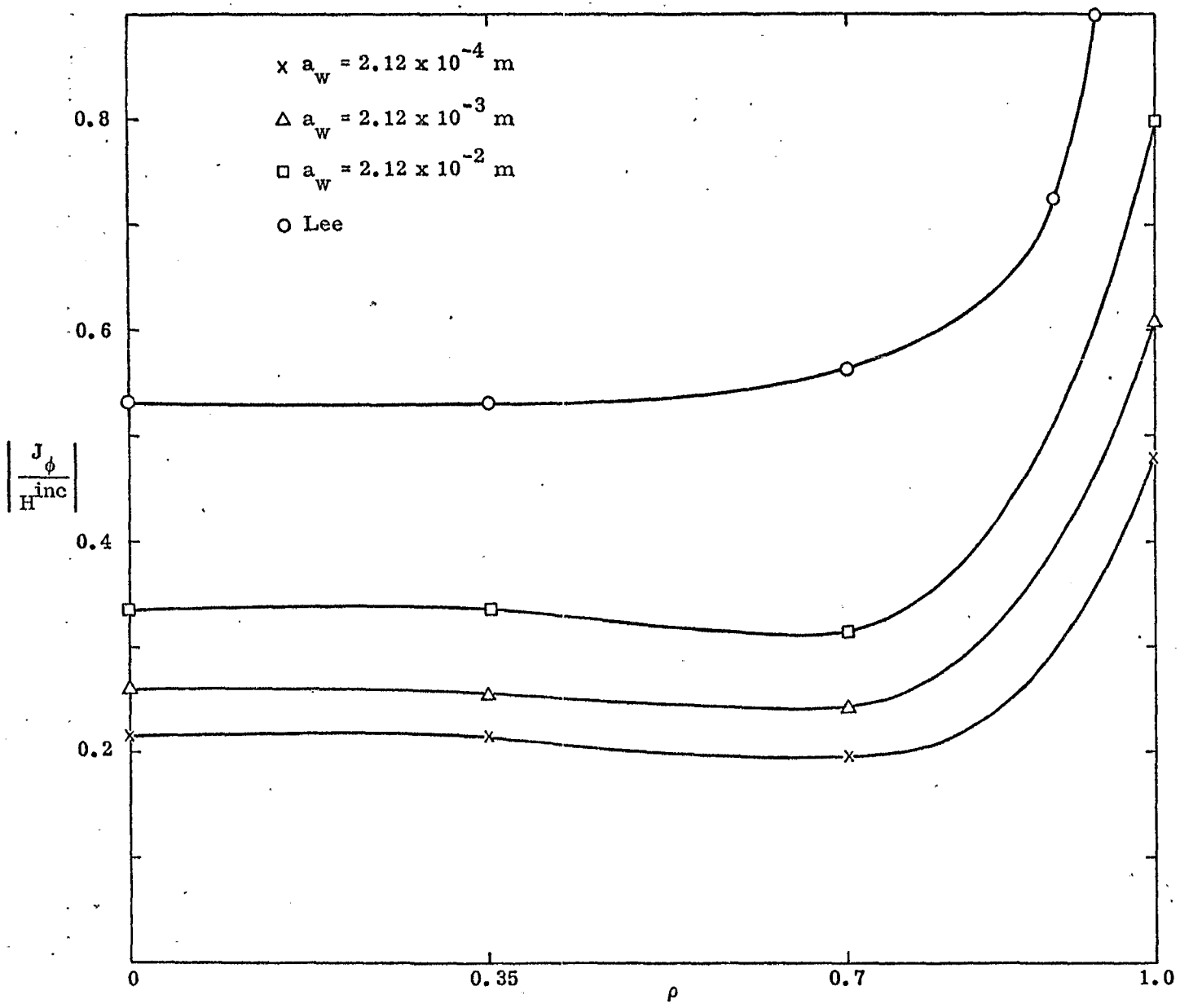

Figure 3. Normalized Azimuthal Current Densities vs Distance from the Center of the Disk of 15 Meters Radius ($\lambda/20$) (λ = 300 meters; ρ is the normalized radius of the disk) for $\phi = \pi/2$

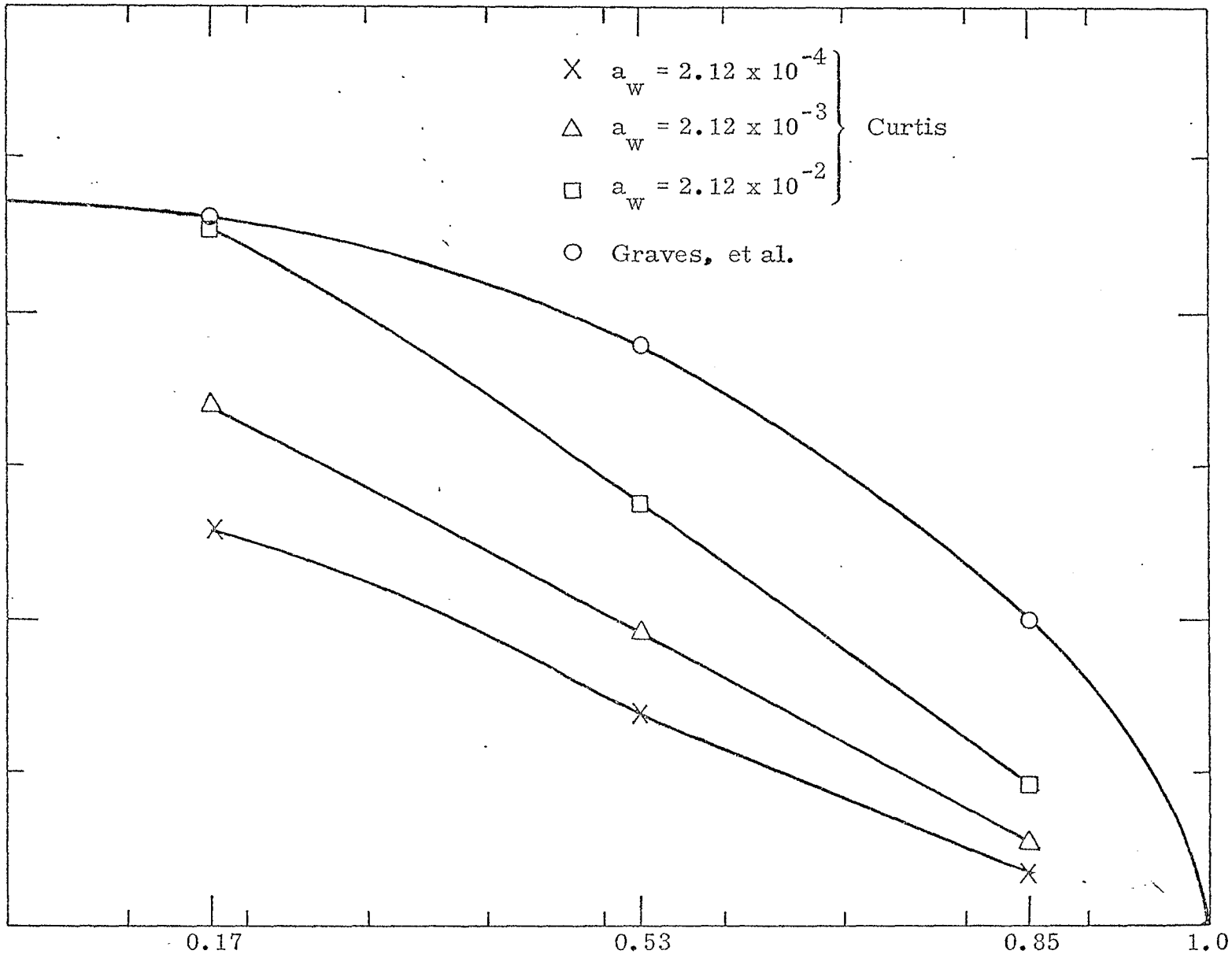

Figure 4. Normalized Radial Current Densities vs Distance from the Center of the Disk of 15 Meters ($\lambda/2$) Radius (λ = 30 meters; ρ is the normalized radius of the disk) for $\phi = 0$

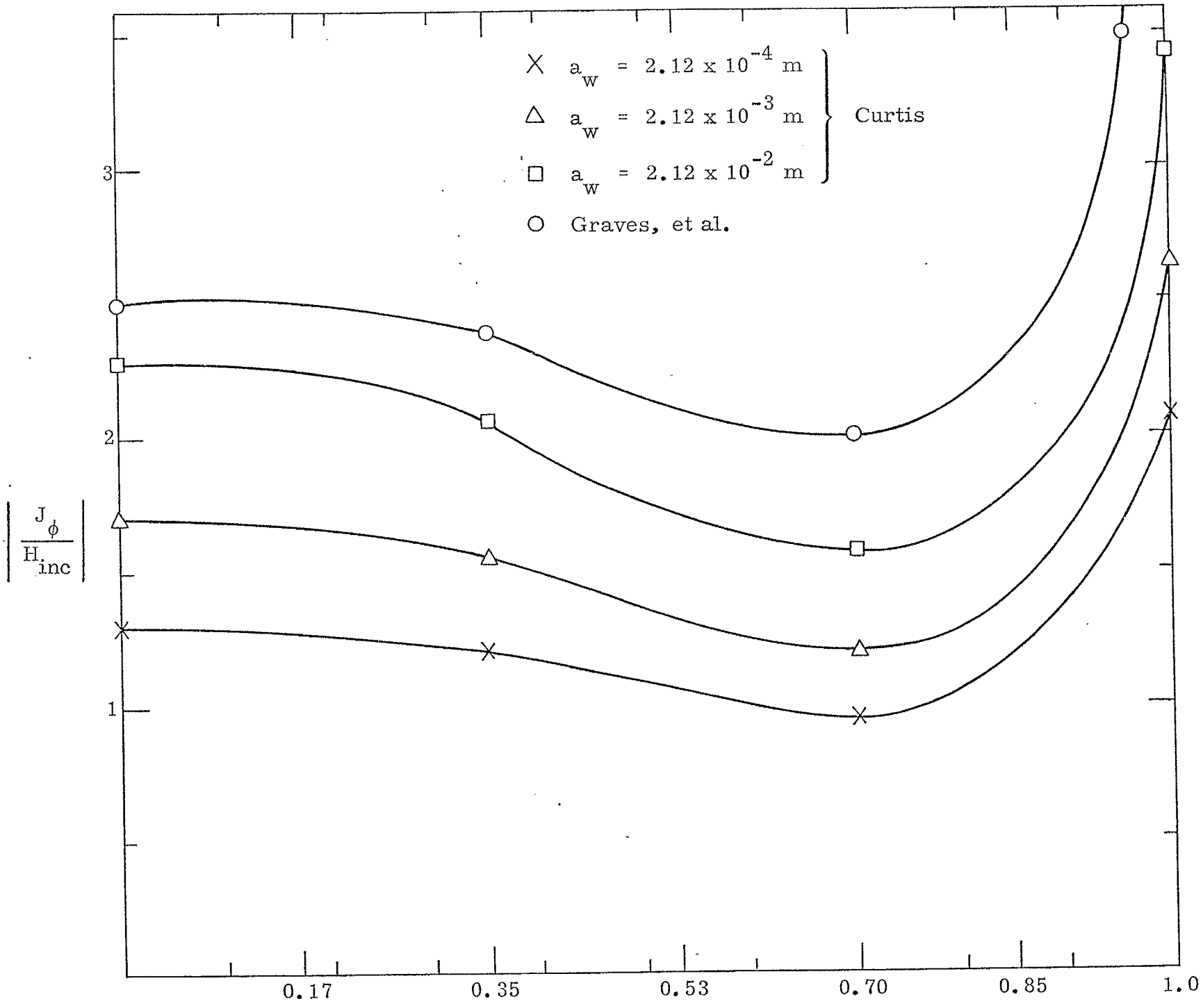

Figure 5. Normalized Azimuthal Current Densities vs Distance from the Center of the Disk of 15 Meters ($\lambda/2$) Radius (λ = 30 meters; ρ is the normalized radius of the disk) for $\phi = \pi/2$

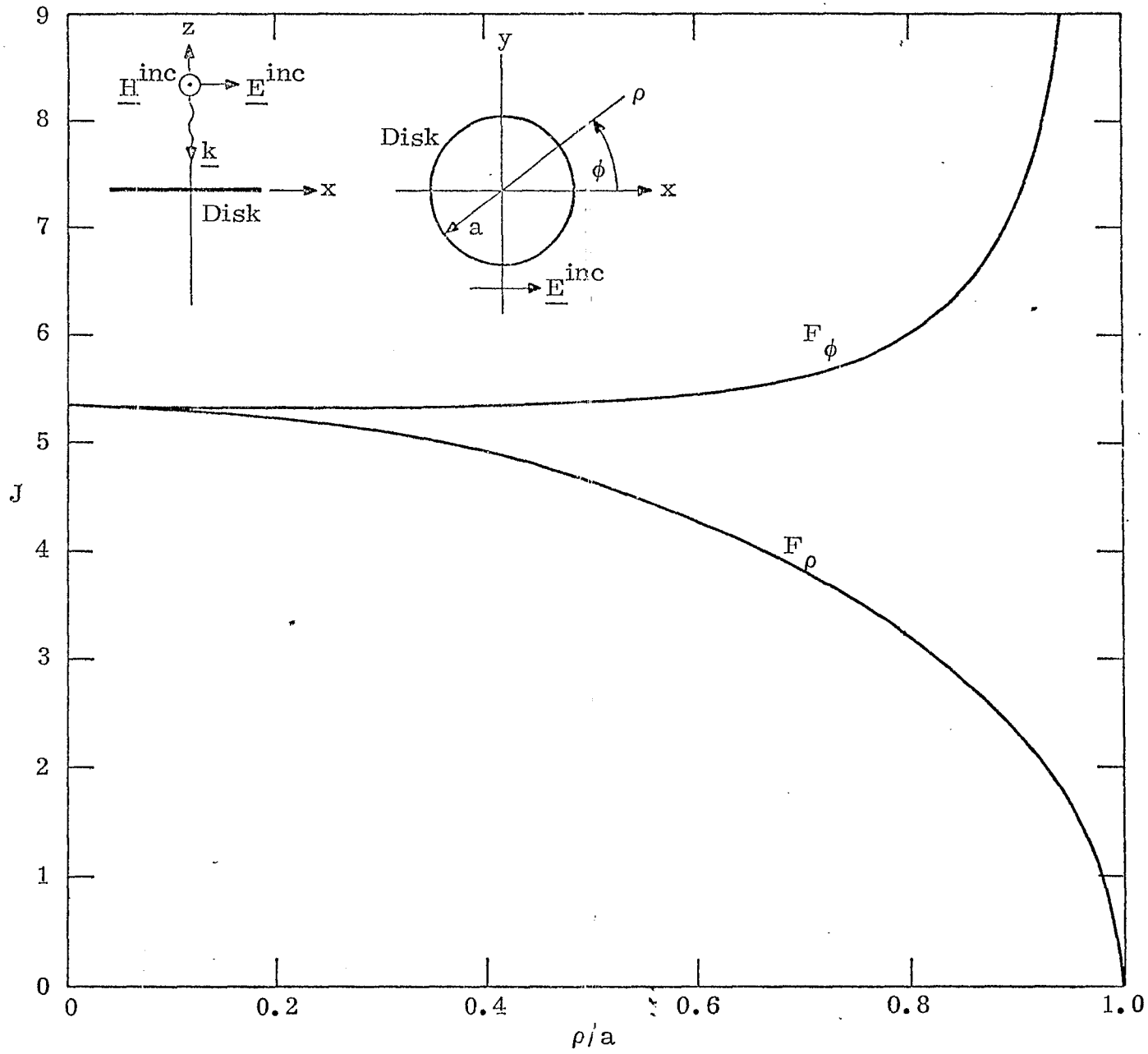

Figure 6. Induced Current Densities on a Small Circular Disk for a Broadside Incidence

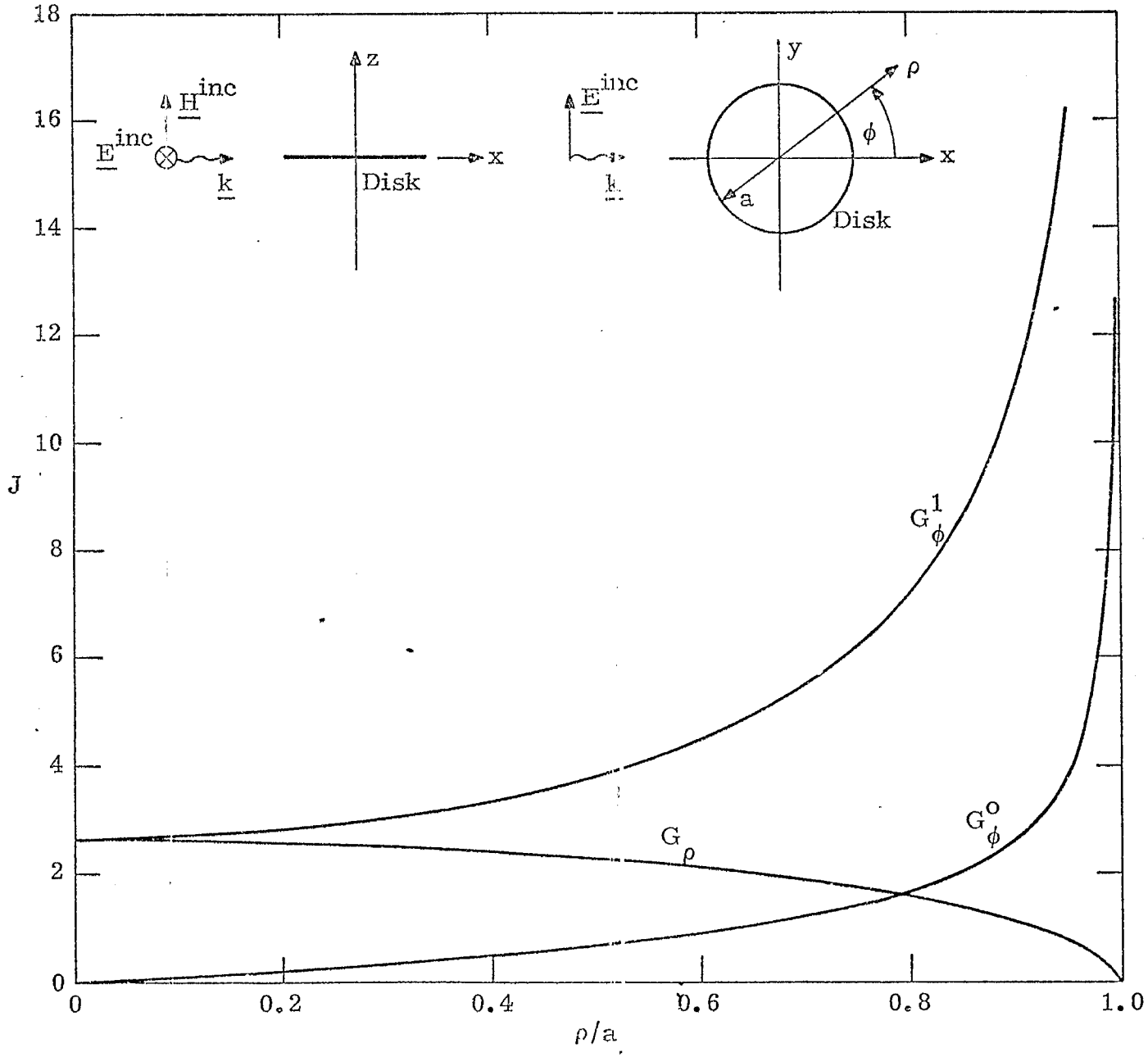

Figure 7. Induced Current Densities on a Small Circular Disk for a Grazing Incidence